

## Can footwall unloading explain late Cenozoic uplift of the Sierra Nevada crest?

George A. Thompson<sup>a\*</sup> and Tom Parsons<sup>b</sup>

<sup>a</sup>*Department of Geophysics, Stanford University, Stanford, CA 94305, USA;* <sup>b</sup>*US Geological Survey, MS-999, 345 Middlefield Rd, Menlo Park, CA 94025, USA*

(Accepted 21 May 2009)

Globally, normal-fault displacement bends and warps rift flanks upwards, as adjoining basins drop downwards. Perhaps the most evident manifestations are the flanks of the East African Rift, which cuts across the otherwise minimally deformed continent. Flank uplift was explained by Vening Meinesz (1950, *Institut Royal Colonial Belge, Bulletin des Séances*, v. 21, p. 539–552), who recognized that isostasy should cause uplift of a normal-faulted footwall and subsidence of its hanging wall. Uplift occurs because slip on a dipping normal fault creates a broader root of less-dense material beneath the footwall, and a narrowed one beneath the hanging wall. In this paper, we investigate the potential influence of this process on the latest stages of Sierra Nevada uplift. Through theoretical calculations and 3D finite element modelling, we find that cumulative slip of about 4 km on range-front faults would have produced about 1.3 km peak isostatic uplift at the ridge crest. Numerical models suggest that the zone of uplift is narrow, with the width controlled by bending resistance of the seismogenic crust. We conclude that footwall unloading cannot account for the entire elevation of the Sierran crest above sea level, but if range-front faulting initiated in an already elevated plateau like the adjacent Basin and Range Province, then a hybrid model of pre-existing regional uplift and localized footwall unloading can account for the older and newer uplift phases suggested by the geologic record.

**Keywords:** Nevadaplano; Sierra Nevada; rift shoulders

### Introduction

It is generally accepted that the Sierra Nevada Block was uplifted and tilted westwards by early Cenozoic time, as evidenced by coarse gold-bearing gravels of the Eocene westward-flowing palaeo-streams (Lindgren 1911). Whether uplift of this ancestral range was renewed in the late Cenozoic, or alternatively whether the magnificent eastern escarpment was formed solely by down-dropping of basins bounding the eastern side is less clear. Recognizing that Basin and Range faulting along the eastern escarpment began about 10 Ma and is continuing, we explore the process of normal-fault unloading of the footwalls of faults that form this escarpment. Is the magnitude of the unloading large enough to produce renewed uplift of the Sierran summit region?

Worldwide, the results of footwall unloading and buoyant (isostatic) uplift seem evident on uplifted margins of plateaus that are bounded by normal faults, including the uplifted shoulders of many rifts. For example, the Colorado Plateau is broadly

---

\*Corresponding author. Email: gathomps@stanford.edu

saucer-shaped; the Wasatch Range forms the plateau's western boundary with the Basin and Range Province. The African Plateau between the uplifted shoulders of the eastern and western rifts forms the shallow basin occupied by Lake Victoria. In that area, Holmes (1944) noted the striking reversal of drainage west of Lake Victoria caused by rapid uplift of hundreds of metres along the western (Lake Albert) rift shoulder. The margins of the Red Sea Rift are similarly uplifted.

Vening Meinesz (1950) and Heiskanen and Vening Meinesz (1958) elucidated normal-fault-block isostasy in Africa. Their purpose was to calculate subsidence of grabens, rise of horsts, and upwarping of plateau margins in an extending terrane. The isostatic response is the result of a narrower buoyant base under grabens, allowing them to subside, and the wider buoyant normal-fault footwalls beneath horsts and plateau margins, causing them to rise or bend up (Figure 1).

The explanation nicely fits the general observations, although complexities such as thermal effects, viscous deep crustal and sub-crustal flow, and erosional transfers of mass were not included; moreover, the response of the elastic upper crust is difficult to evaluate. We note that, as in all isostatic support of topographic relief, a strong upper layer overlying a yielding lower crust or mantle is required. It is the strong upper layer that distributes lateral and vertical support. Heiskanen and Vening Meinesz (1958) treated the entire crust as the strong layer overlying a viscous mantle, but seismic imaging of the Basin and Range crust demonstrates faulting of the upper crust with little or no perturbation of the crust–mantle boundary beneath fault blocks (Klemperer *et al.* 1986 and many later studies). For modelling purposes, we take the upper crust to be the seismogenic layer, about 15 km thick, overlying a viscous lower crust and upper mantle.

### **Background: the Sierra Nevada**

The modern Sierra Nevada is generally viewed as a semi-rigid block gently tilted to the west and bounded on the east by spectacular escarpments created by late Cenozoic normal faults of the encroaching Basin and Range Province. Since the work of Lindgren (1911) on the Eocene gold-bearing gravels, it has been recognized that the exhumed westward-draining channels are steeper than the modern river channels. This observation led to the interpretation that the ancient channels were steepened by westward tilting of the Sierra Nevada Block at the time of late Cenozoic faulting of the eastern front (Wakabayshi and Sawyer 2001 and references therein). Alternatively, the Sierra Nevada may have been high since Eocene time and may have formed the western slope of a high plateau ('Nevadaplano'), analogous to the Altiplano of South America until it was disrupted by Basin and Range faulting in the late Cenozoic (e.g. Mulch *et al.* 2006; Crowley *et al.* 2008; Cassel *et al.* 2009; Henry 2009; Van Buer *et al.* 2009). In the Nevadaplano interpretation, faulting along the Sierran front might have produced only depression of the basins (relative to sea level) or, additionally, the faulting may have caused renewed uplift of the Sierran summit.

In particular, the reconstructed ancient river channels draining westwards across the Sierra from the plateau to the east and the isotopic evidence of high elevation in the Oligocene channel deposits, all nicely summarized by Henry (2009), provide convincing evidence for a high ancestral Sierra Nevada and a high plateau to the east. Recognizing however, that the isotopic sampling necessarily followed the old channels and mountain passes that may not represent mean elevation of the Sierran summit, we suggest that a case may be made for incremental late Cenozoic uplift. Moreover, the structure of the eastern escarpment of the Sierra Nevada varies along strike from comparatively simple large

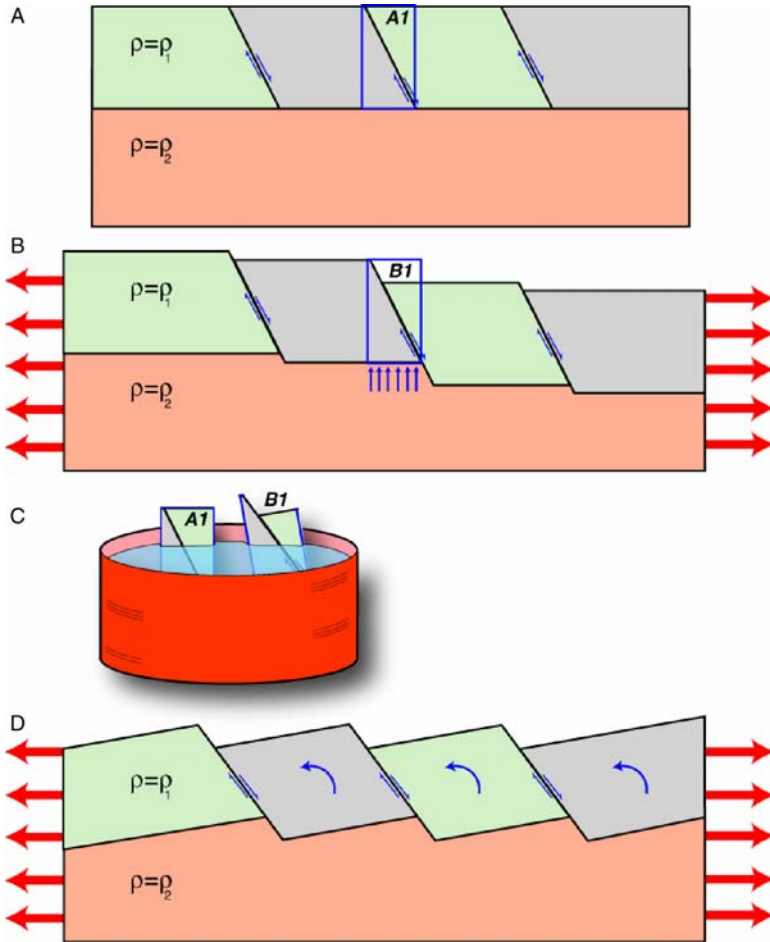


Figure 1. (a) Normal-faulted crust overlies and ‘floats’ in a ductile substrate, where  $\rho_1 < \rho_2$ ; (b) under extension, hanging walls slide down and unload footwalls. If we compare the mass within same-sized boxes attached to the top of the footwalls, where box *A1* is before fault slip, and box *B1* is after fault slip, we note that box *B1* is lighter, because some mass has slipped away; (c) if we could float boxes *A1* and *B1* in a fluid, then the lighter box *B1* would ride higher and tilt; (d) in the simplest case of rigid blocks, the isostatic result of normal faulting is block rotation. In the real crust, it is more likely that wider blocks would bend up as a result of isostatic forces.

normal faults along the highest escarpments to warping and distributed faulting along lower stretches (Thompson and White 1964). We evaluate the expected uplift caused by Basin and Range faulting, first by means of a conceptual semi-quantitative analogue model of the buoyancy, and second by means of a more comprehensive numerical model. These two approaches are designed to clarify and quantitatively evaluate the process.

### *Conceptual model*

While recognizing that the Sierra Nevada probably existed as a high range since early Cenozoic time, we infer that the summit region received a late Cenozoic boost owing to footwall unloading of the Basin and Range normal faults that form the great escarpment of

the eastern front. We do not necessarily infer that the entire Sierra Nevada microplate was subjected to renewed tilting as a rigid plate but rather that the summit region may have been bent up, analogous to the warped margins of the African Plateau and the Colorado Plateau. Such warping can be accomplished in a rigid block by innumerable minor movements on small faults, fractures, and joints, as Compton (1966) convincingly demonstrated in granitic rocks underlying compressional folds in sedimentary strata. Moreover, many small, active faults, demonstrating non-rigid behaviour of the Sierran Block, are known on the western slopes (Wakabayshi and Sawyer 2001). To roughly quantify the conceptual model with an observed analogue, we turn to a well-documented example north of the Sierra Nevada.

Because the Sierra Nevada lacks continuous, dated, stratigraphic markers that would allow us to quantify deformation, we focus on an analogous region along the western boundary of the Basin and Range Province, the Surprise Valley Fault bounding the uplifted Modoc Plateau in northeastern California (Lerch *et al.* 2009). Geologic data and seismic imaging indicate that, as late Cenozoic faulting progressed on the Surprise Valley Fault, the footwall strata warped upwards about  $25^\circ$ , and the fault dip was simultaneously reduced by this amount. Dip slip is estimated from the seismic image as about 9 km, or possibly less because of uncertainties in seismic velocity in basin fill. We estimate up-warp as roughly 2.5 km at the restored summit, and erosion has reduced this by about 1.5 km, making the net gain in elevation roughly 1 km. We interpret the warping as caused by footwall unloading and test this inference by isostatic calculations.

Mass removal on the footwall is proportional to cross-sectional area of the unloaded mass (estimated on the Lerch *et al.* (2009) cross-section with erosion restored) multiplied by density. This mass consists of direct surface displacement of the hanging wall off the footwall plus erosional unloading, which consists of about half the direct effect. Additional unloading consists of subsurface replacement of the original rock in the hanging wall by lower-density basin fill, but this estimated effect is small enough to be neglected in view of other uncertainties. We take the density of the volcanic pile in the footwall to be  $2.4 \times 10^3 \text{ kg m}^{-3}$  and the density of inflowing lower crustal rocks to be  $2.8 \times 10^3 \text{ kg m}^{-3}$ . The result is a mean uplift of about 2.5 km over a plateau breadth of 10 km (or a greater uplift over a narrower breadth). Allowing for erosion of about 1.5 km, the calculated uplift is in rough agreement with the observed elevation.

The result tends to be maximized by assigning no resistance to flow in the compensating masses and no resistance to bending of the upper plate, although these conditions might be approached in the long course of geologic time. Moreover, compared with typical Sierran frontal faults in central California, the Surprise Valley Fault (ca. 9 km of dip slip) is larger and has a much lower dip (ca.  $35^\circ$ ). Scaling down the result by a factor of two or three, to represent 3 or 4 km of dip slip on Sierran frontal faults, seems appropriate. This would suggest 0.8–1.2 km of uplift caused by footwall unloading, and erosion would reduce the increase in elevation.

### A 3D finite element simulation of range-front footwall uplift

To further assess the role of footwall unloading on range-front uplift, we construct a 3D finite element model to simulate extending crust. The purpose of the model is to roughly quantify expected flank uplift resulting from slip on a dipping normal fault and its accompanying isostatic unloading, while taking into account frictional and crustal bending resistance. This numerical model, while still theoretical, is less idealized than the initial concept by Vening Meinesz (1950). The model has a 15 km-thick elastic crust floating in a

thicker (85 km) ductile layer (Figure 2). Thickness of the ductile layer does not affect results provided it is thick enough to absorb elevation changes of the elastic layer above.

The elastic part of the crust (upper 15 km) is simulated with eight-node, tetrahedral elements (Figure 2). The constitutive properties of the crust are approximated by those of wet Westerly granite, and characterized by three elastic parameters: a Young modulus of  $E = 8 \times 10^4$  MPa, a density of  $\rho = 2.8 \times 10^3$  kg m<sup>-3</sup>, and a Poisson ratio of  $\sigma = 0.25$ . Solid model elements had special properties intended for replicating rock behaviour. If stress concentrations exceed strength criteria as determined from laboratory studies (Birch 1966; Christensen 1996), elements can respond by cracking or crushing. Orientations of fracture planes are determined by magnitudes and directions of principal stress axes and the coefficient of internal friction for granite ( $\mu = 0.6$ ) (Byerlee 1978) (Figure 3). Element fracturing is an essential mechanism that enables the elastic layer to bend through permanent, macro-scale plastic deformation, preventing unrealistically large elastic strain accumulation. A model with an unbreakable elastic upper layer would either rotate if its edges were unconstrained, or accumulate very large elastic stresses with a bending moment dependent on its length measured from its fixed boundary.

The crustal part of the finite element model has a 60° dipping cut in it that represents a major range-front fault (Figure 2). The fault is deformable, and is constructed from contact elements that obey the Coulomb failure relation

$$CF \equiv \bar{\tau}_f + \mu(\sigma_n), \quad (1)$$

where  $\tau$  is shear stress acting on a fault surface,  $\mu$  is the friction coefficient, and  $\sigma_n$  is the component of stress acting normal to a fault surface (pore fluid pressures were assumed constant and hydrostatic). We use a low friction coefficient of  $\mu = 0.2$ ; this parameter controls the amount of shear stress carried by the fault and has little effect on the results because we allow the fault to slip at steady state, simulating many earthquake cycles. A higher friction coefficient means the fault could resist a few additional metres of slip. Contact elements have zero thickness and are welded to the sides of the solid model elements. The modelled range-front fault passes through the upper 15 km of the model,

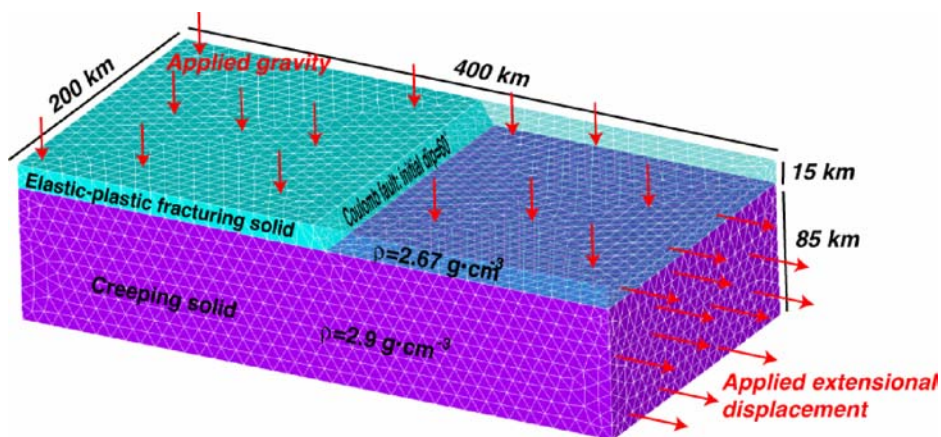


Figure 2. 3D finite element model geometry. An elastic-plastic upper crust floats in a ductile, creeping lower-crust and upper mantle. A 60° dipping fault cuts through the upper crust, and slips when the model's eastern edge is displaced in extension. We use the model to investigate and quantify the role of footwall unloading on range-front uplift.

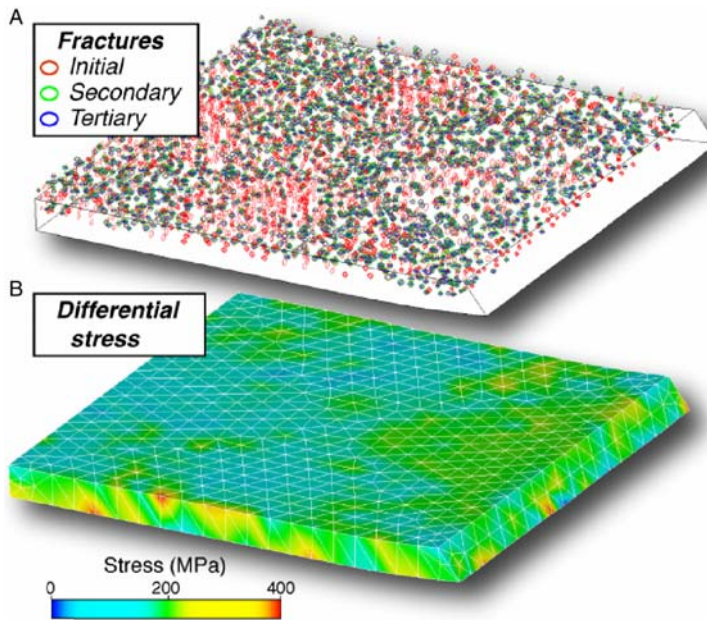


Figure 3. (a) A portion of the finite element model upper crustal layer shown with element fracture planes that respond to applied extension, and isostatic bending of the crust from fault slip. Fractures interact and can develop secondary orientations resulting from developing stress changes in the model. Quasi-plastic deformation by elastic fracturing acts to prevent large stress concentrations in the elastic layer as shown by the differential stress accumulation in (b), which does not exceed 400 MPa, and much less in most of the volume. A fractured crust is a closer approximation to the real Earth than an unbreakable elastic solid.

defining two adjacent blocks. The fault is allowed to extend another 15 km into the ductile layer beneath to prevent sudden termination of strain at the base of the elastic upper crust.

The model free surface is unconstrained, and is initially flat, which approximates a Nevadaplano starting point. The west edge is restrained in the east–west direction, and the north and south model edges are constrained not to move in the north–south directions. The base of the model is allowed to flow freely in the horizontal directions, but is fixed in the vertical. There are no other vertical constraints on the model apart from gravitational loading.

Simulation of flank uplift begins by establishing an initial isostatic balance under gravity. The model is then stretched by gradual displacement of the eastern edge until it is extended by 10%. Much of the extensional strain in the upper crustal layer is accomplished by slip on the central normal fault, which generates about 4 km of total offset (Figure 4), and the balance is accomplished by small fractures (Figure 2). As the fault slips in the model, the footwall becomes increasingly unloaded; the resulting isostatic effect causes about 1200–1300 m of uplift through bending of the range front that is concentrated within a 70–100-km-wide zone parallel to the fault. A comparable subsidence occurs on the hanging wall of the fault, where a ~1200–1500 m deep basin is produced in the model (Figure 4).

We compare our 3D finite element model with the Sierra Nevada range, and see some basic features in common (Figure 4). In our model we have a single range front fault with about 4 km of slip, whereas the Sierra Nevada uplift is accomplished through multiple, closely spaced normal faults with comparable cumulative slip (Ramelli *et al.* 1999;

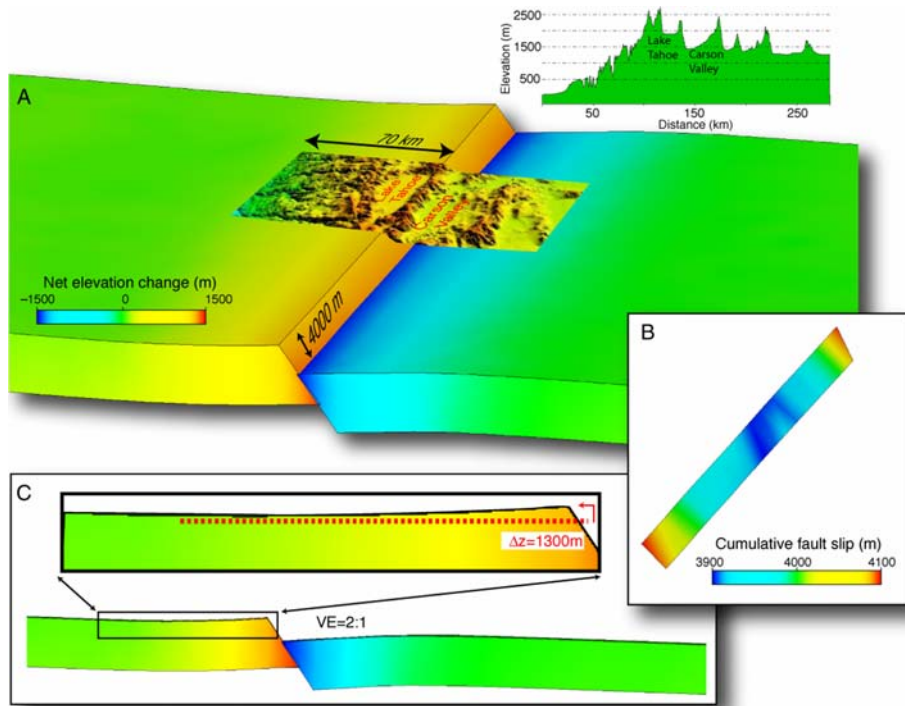


Figure 4. Results of 3-D finite element modelling of range-front fault uplift. (a) Vertical change in the model resulting from (b)  $\sim 4$  km slip on the  $60^\circ$  dipping normal fault. (c) A cross-section view shows about 1300 m of uplift resulting from isostatic bending of the footwall. Comparable subsidence of the hanging wall is also evident in the model. A topographic profile across the central Sierra Nevada range is shown for comparison purposes.

Brothers *et al.* 2009; Dingler *et al.* 2009). We find that the predicted footwall uplift of  $\sim 1300$  m cannot account for the total elevation of the Sierra front, which averages 2500–3000 m above sea level. However, the 1300 m we calculate can account for the difference in elevation between the Sierran front and the adjacent Basin and Range Province, which averages 1100–1500 m above sea level. Therefore, if range-front faulting initiated within an already elevated plateau, then the present Sierran crest can be explained by isostatically driven uplift caused by footwall unloading and collapse of the adjacent Basin and Range Province.

## Conclusions

Clearly, the late Cenozoic encroachment of Basin and Range normal faulting on the eastern front of the Sierra Nevada was capable of producing renewed uplift of the Sierran summit. The magnitude of the expected uplift is many hundreds of metres to more than a kilometre for typical normal-fault displacements in the central California part of the range. Although the elevation gain might initially have been reduced by erosion, this unloading would be expected to produce renewed isostatic uplift that would recover most of the elevation loss.

The interpretation of renewed late Cenozoic uplift of the Sierran summit caused by normal faulting is greatly reinforced by worldwide comparisons. The process appears to be general. Plateau margins bounded by normal faults are warped up by unloading of the fault footwalls and related processes.

## Acknowledgements

We thank many students and colleagues for helpful discussions, and Simon Klemperer and Norm Sleep for their critical reviews.

## References

- Birch, F., 1966, Compressibility; elastic constants: Geological Society of America Memoir, v. 97, p. 97–173.
- Brothers, D.S., Kent, G.M., Driscoll, N.W., Smith, S.B., Karlin, R., Dingler, J.A., Harding, A.J., Seitz, G.G., and Babcock, J.M., 2009, New constraints on deformation, slip rate, and timing of the most recent earthquake on the West Tahoe-Dollar Point Fault, Lake Tahoe Basin, California: Bulletin of the Seismological Society of America, v. 99, p. 499–519, DOI: 10.1785/0120080135.
- Byerlee, J.D., 1978, Friction of rocks: Pure and Applied Geophysics, v. 116, p. 615–626.
- Cassel, E.J., Graham, S.A., and Chamberlain, C.P., 2009, Cenozoic tectonic and topographic evolution of the northern Sierra Nevada, California, through stable isotope paleoaltimetry in volcanic glass: Geology, v. 37, p. 547–550, DOI: 10.1130/G25572A.1.
- Christensen, N.I., 1996, Poisson's ratio and crustal seismology: Journal of Geophysical Research, v. 101, p. 3139–3156.
- Compton, R.R., 1966, Analyses of Pliocene-Pleistocene deformation and stresses in northern Santa Lucia Range, California: Geological Society of America Bulletin, v. 77, p. 1361–1379.
- Crowley, B.E., Koch, P.L., and Davis, E.B., 2008, Stable isotope constraints on the elevation history of the Sierra Nevada Mountains, California: Geological Society of America Bulletin, v. 120, p. 588–598, DOI: 10.1130/B26254.1.
- Dingler, J., Kent, G., Driscoll, N., Babcock, J., Harding, A., Seitz, G., Karlin, B., and Goldman, C., 2009, DOI: 10.1130/B26244.1 A high-resolution seismic CHIRP investigation of active normal faulting across the Lake Tahoe Basin, California-Nevada: Geological Society of America Bulletin, v. 121.
- Heiskanen, W.A., and Vening Meinesz, F.A., 1958, Faulting and Graben development as a consequence of Uniaxial Stress Release in the Crust, 390–394, The Earth and its Gravity Field: New York: McGraw Hill, 470 pp.
- Henry, C.D., 2009, Uplift of the Sierra Nevada, California: Geology, v. 37, p. 575–576, DOI: 10.1130/focus062009.1.
- Holmes, A., 1944, Principles of Physical Geology: Edinburgh: Thomas Nelson and Sons.
- Klemperer, S.L., Hauge, T.A., Hauser, E.C., Oliver, J.E., and Potter, C.J., 1986, The Moho in the northern Basin and Range, Nevada, along the COCORP 40 N seismic-reflection transect: Geological Society of America Bulletin, v. 97, p. 603–618.
- Lerch, D.W., Klemperer, S.L., Egger, A.E., Colgan, J.P., and Miller, E.L., 2009, The northwestern margin of the Basin-and-Range Province, part 1: reflection profiling of the moderate-angle (~30°) Surprise Valley Fault: Tectonophysics, DOI: 10.1016/j.tecto.2009.05.028.
- Lindgren, W., 1911, The Tertiary gravels of the Sierra Nevada of California: U.S. Geological Survey Professional Paper, v. 73, p. 1–226.
- Mulch, A., Graham, S.A., and Chamberlain, C.P., 2006, Hydrogen isotopes in Eocene River gravels and paleoelevation of the Sierra Nevada: Science, v. 313, p. 87–89.
- Ramelli, A., Bell, J.W., dePolo, C.M., and Yount, J.C., 1999, Large-magnitude, late Holocene earthquakes on the Genoa Fault, west-central Nevada and eastern California: Bulletin of the Seismological Society of America, v. 89, p. 1458–1472.
- Thompson, G.A., and White, D.E., 1964, Regional geology of the Steamboat Springs area, Washoe County, Nevada: U.S. Geological Survey Professional Paper, v. 458A, p. A1–A52.
- Van Buer, N.J., Miller, E.L., and Dumitru, T.A., 2009, Early Tertiary paleogeologic map of the Northern Sierra Nevada batholith and the northwestern Basin and Range: Geology, v. 37, p. 371–374, DOI: 10.1130/G25448A.1.
- Vening Meinesz, F., 1950, Les grabens africains, résultat de compression ou de tension dans la croûte terrestre?: Institut Royal Colonial Belge, Bulletin des Séances, v. 21, p. 539–552.
- Wakabayshi, J., and Sawyer, T.L., 2001, Stream incision, tectonics, uplift, and evolution of topography of the Sierra Nevada, California: Journal of Geology, v. 109, p. 539–562.